The Voltage-dependent Calcium Channel β Subunit Contains Two Stable Interacting Domains*

Yarden Opatowsky‡, Orna Chomsky-Hecht‡, Myoung-Goo Kang§, Kevin P. Campbell§¶, and Joel A. Hirsch‡‖

From the ‡Department of Biochemistry, Faculty of Life Sciences, Tel Aviv University, Sherman Bldg., Rm. 621, Ramat Aviv 69978, Israel and the §Department of Physiology and Biophysics, Howard Hughes Medical Institute, Carver College of Medicine, University of Iowa, Iowa City, Iowa 52242-1101

Voltage-dependent calcium channels selectively enable Ca^{2+} ion movement through cellular membranes. These multiprotein complexes are involved in a wide spectrum of biological processes such as signal transduction and cellular homeostasis. α_1 is the membrane pore-forming subunit, whereas β is an intracellular subunit that binds to α_1, facilitating and modulating channel function. We have expressed, purified, and characterized recombinant β_3 and β_{2a} using both biochemical and biophysical methods, including electrophysiology, to better understand the β family's protein structural and functional correlates. Our results indicate that the β protein is composed of two distinct domains that associate with one another in a stable manner. The data also suggest that the polypeptide regions outside these domains are not structured when β is not in complex with the channel. In addition, the β structural core, comprised of just these two domains without other sequences, binds tightly to the α interaction domain (AID) motif, a sequence derived from the α_1 subunit and the principal anchor site of β. Domain II is responsible for this binding, but domain I enhances it.

Voltage-dependent calcium channels (VDCCs)[1] permit the flow of Ca^{2+} ions through cellular membranes as a function of membrane potential. These protein complexes are central components in a variety of physiological systems of organisms, ranging from yeast to human. They play pivotal roles in signal transduction and homeostasis processes.

Functional roles for these channels vary based on cell type. In muscle, both skeletal and cardiac, the predominant VDCCs ($Ca_V1.1$ and $Ca_V1.2$) cause release of Ca^{2+} into the cytosol from intracellular stores, thereby initiating contraction (1, 2). In neurons and endocrine cells, neurotransmitter or hormone secretion requires VDCC activity. In addition, electrical activity,

specifically the action potential in cardiac myocytes, is regulated by VDCCs. Finally, calcium influx and concentration controlled by VDCCs plays a significant role in neuronal gene expression (3). Pathways have been elucidated, where for one example, VDCC activity gives rise to phosphorylation of CREB, a transcription factor (4), thereby activating transcription of a myriad of target genes.

The VDCC comprises four distinct polypeptides: α_1, $\alpha_2\delta$, β, and γ (5). α_1 is the membrane pore-forming subunit and numbers between 1800 and 2400 residues in length. Its sequence exhibits repeats comprising four transmembrane modules or domains, akin to the tetrameric architecture of potassium channels. Each module contains the canonical transmembrane arrangement for voltage-gated ion channels *i.e.* six transmembrane segments. Modules are connected by linkers that are located in the intracellular milieu, as are both the N and C termini. The high voltage-activated channel subunits, $Ca_V1.x$ and $Ca_V2.x$ (α_1), numbering seven in total, share a high degree of sequence similarity but nevertheless encode distinct electrophysiological activities.

The β subunit was first isolated biochemically in tight association with α_1 (6). Four isoforms have been discovered, ranging in size from 52 to 78 kDa (7). The lack of a transmembrane region suggested that β very likely interacts with the channel through one of the intracellular domains of α_1. Campbell and coworkers (8) found such a region in the linker between repeats I and II of the α_1 subunit. The data indicate that α_1 and β subunits interact directly with each other with a stoichiometry of 1:1 (9). β also interacts with other regions of α_1 (10–14), depending on the isoform, but the region discovered by Campbell and coworkers appears to be the primary, high affinity site of interaction.

The electrophysiological function of the β subunit is a modulatory one (15–17). It increases VDCC peak current amplitude from 10- to 18-fold depending on the channel type. Furthermore, β accelerates channel activation, modifies inactivation kinetics, and shifts the voltage-dependence of the channel (18). It has been convincingly shown that β acts by both chaperoning VDCCs to the membrane and modulating gating (19–21). The diverse β isoforms have quantitatively different effects on the various electrophysiological parameters. These isoform differences suggest a mechanism for the cellular specificity of VDCC activity through combinatorial permutations of different β isoform subunits associating with different α_1 isoforms. Nevertheless, the molecular mechanism of the β subunit remains unclear. Protein-protein interactions, which have been mapped to a minimum of 18 residues in the α_1 module I–II linker described above, dubbed the AID (α interaction domain), and a 30-residue sequence in VDCC β, dubbed the BID (β interaction domain), play a critical role (8, 22).

[1] The abbreviations used are: VDCC, voltage-dependant calcium channel; AID, α_1 interacting domain; BID, β interacting domain; IPTG, isopropyl-1-thio-β-D-galactopyranoside; TEV, tobacco etch virus; βME, β-mercaptoethanol; HPLC, high-pressure liquid chromatography; CD, circular dichroism; MALDI-MS, matrix-assisted laser desorption ionization-mass spectrometry; PB, protein buffer; WT, wild type.
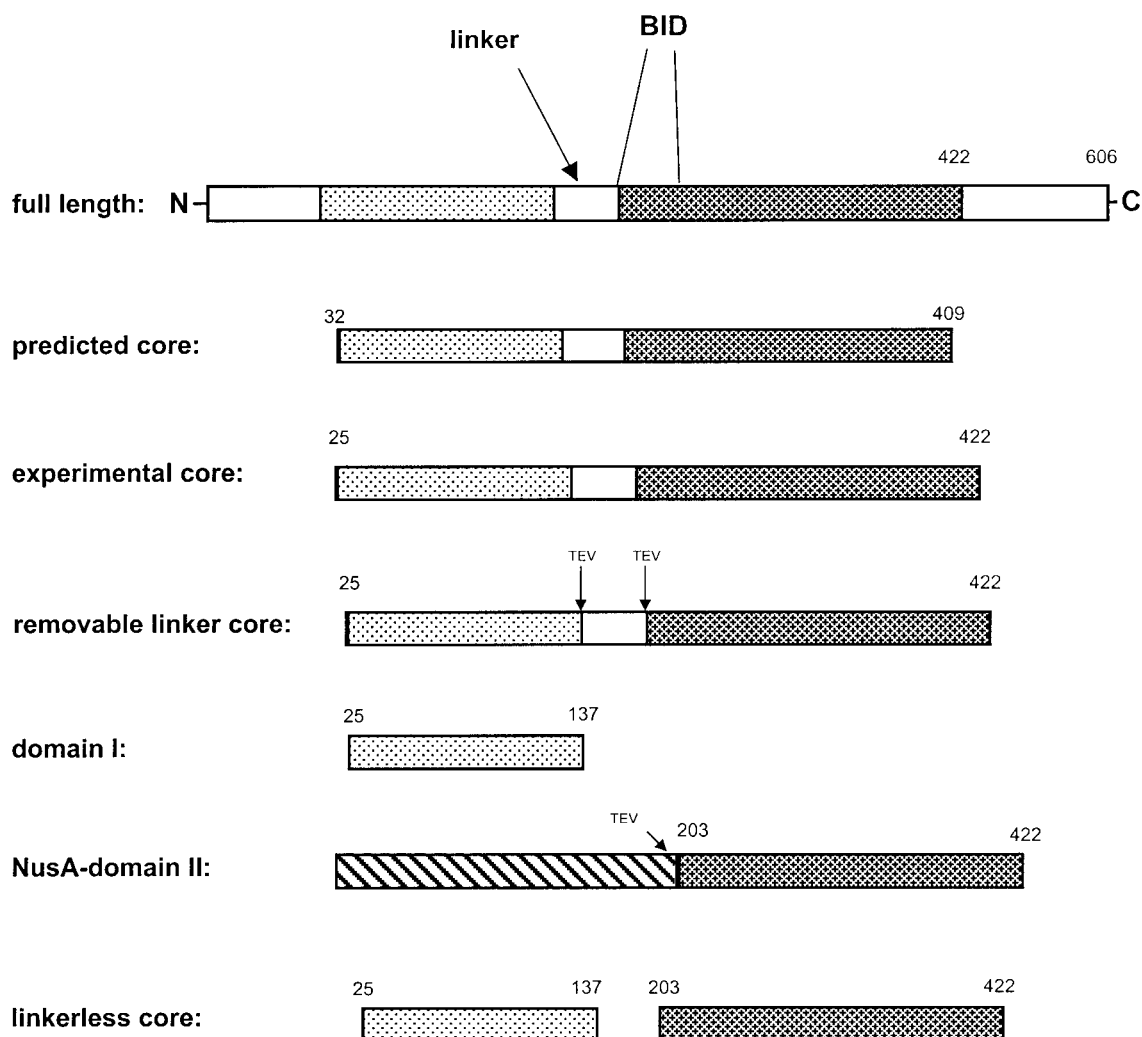
FIG. 1. **Schematic of the rabbit VDCC β_{2a} primary sequence, a representative of the β family, and the various constructs prepared in this study.** The *lightly stippled box* denotes the first conserved domain, domain I, and the *darkly stippled box* denotes the second conserved domain, domain II. The BID, a sequence responsible for binding to VDCC α_1, is located as shown in the beginning of domain II.

Although, considerable attention has been paid to VDCC β, especially on the functional level, little experimental data is available concerning the protein's tertiary structure. Cloning and sequencing of the various β isoforms from a spectrum of species showed that two sequence regions were fairly conserved (Fig. 1). Based on the identification of these regions, structure-function analyses have shown that much of the functional activity associated with VDCC β resides in these two regions (22). Subsequently, bioinformatic analysis, including molecular modeling studies, proposed that these two regions have structural similarity to SH3 and guanylate kinase folds (23). Here, we describe experimental studies of the VDCC β protein, which give insight into the domain structure of the protein and the interaction between those domains, as well as correlate this data with functional biochemistry and electrophysiology.

EXPERIMENTAL PROCEDURES

Subcloning, Expression, and Purification of VDCC β_3 Subunit—Recombinant rat VDCC β_3 subunit (M88751) was expressed in *Escherichia coli* strain BL-21 Tuner (Novagen), containing the "RIL" Codon Plus™ plasmid (Stratagene), using a modified pET21 (Novagen) vector (an His_8 and TEV protease site were engineered between the NcoI and BamHI sites of pET21d, a gift of Dr. Sean Juo). The protein was purified by sequential metal-chelate, ion-exchange, and hydroxylapatite chromatography.

PCR was used to engineer EcoRI and BamHI restriction sites into the β_3 gene. The oligonucleotide primers used for amplification of the β_3 gene from the original plasmid were the following: sense primer A, 5′-GCGCGGATCCTATGACGACTCCTACGTCCCC; antisense primer B, 5′-GCGCGGATCCTATGACGACTCCTACGTGCCC. PCR product was ligated into doubly digested (EcoRI and BamHI) pET21d vector. Positive clones were identified by restriction analysis and subsequently sequenced.

Transformed Tuner cells were grown for 3–4 h at 37 °C in 10 liters of LB media, containing 100 μg/ml ampicillin, and 34 μg/ml chloramphenicol. Upon reaching an A_{600} of 0.3, the temperature was lowered to 16 °C, and growth continued until the culture reached an A_{600} of 0.6. Protein expression was induced with 200 μM IPTG. Cells were harvested after 14 h by centrifugation, frozen, and suspended in 100 ml of lysis buffer, buffer L (300 mM NaCl, 50 mM sodium phosphate (pH 7), 1 mM phenylmethylsulfonyl fluoride, 5 mM $MgCl_2$, 0.2% Triton X-100, 1 mM βME, 10 mg of lysozyme, 1 mg of DNase). After lysis by French pressure cell (Aminco), cell debris was removed by centrifugation at 20,000 $\times$ g. The soluble fraction was loaded onto a pre-equilibrated metal chelate "Talon" (Clontech) column (buffer A: 300 mM NaCl, 50 mM sodium phosphate, pH 7), at a flow rate of 1.5 ml/min. The column was washed with buffer A, containing 5 mM imidazole, until a stable base line was achieved. After elution with buffer A, supplemented with 150 mM imidazole, the protein eluate was then diluted 3-fold with water and loaded onto a pre-equilibrated Source-Q (Amersham Biosciences) column (buffer Q: 70 mM NaCl, 20 mM sodium phosphate, pH 7). The column was then washed with buffer Q, and fractions were eluted with a shallow linear gradient of buffer Q, containing 70–300 mM NaCl. VDCC β_3-containing fractions were pooled (130–150 mM NaCl) and diluted 2-fold in 600 mM NaCl to buffer H concentrations (10 mM phosphate buffer (pH 7) and 300 mM NaCl) and subjected to TEV

protease prepared in house according to a previous study (24). The proteolysis continued for 12 h. Subsequently, the sample was loaded onto a pre-equilibrated (with H buffer) hydroxylapatite (Calbiochem) column and eluted with a linear gradient of H buffer 10–100 mM potassium phosphate, pH 7 (eluted at 50 mM potassium phosphate). Pooled fractions were concentrated to 10 mg/ml using spin concentrators (Vivascience), divided into aliquots, and flash frozen in liquid N_2.

Subcloning, Expression, and Purification of VDCC β_{2a} Subunit—PCR was used to engineer EcoRI and BamHI restriction sites into the VDCC β_{2a} (X64297) gene. The oligonucleotide primers used for amplification of the new β_{2a} gene from the original plasmid were the following: sense primer C, 5′-GCGCGGATCCCTTGACAGGCACCTCGCGG-C-3′; antisense primer D, 5′-CGCCGAATTCTCATTGGCGGATGTA-3′. Subsequent subcloning was as described for VDCC β_3.

The VDCC β_{2a} subunit was expressed as for β_3. Purification was as follows. The soluble fraction of the crude extract was loaded on a pre-equilibrated Ni-CAM column (Sigma) (buffer B: 50 mM sodium phosphate (pH 8) and 300 mM NaCl) and washed with buffer B, containing 5 mM imidazole. The protein was then eluted with buffer B, containing 150 mM imidazole, and diluted 6-fold, followed by loading onto a pre-equilibrated Q-Sepharose (Amersham Pharmacia) column (buffer C: 20 mM sodium phosphate (pH 8), 40 mM NaCl, 5 mM βME). Fractions were eluted with a shallow linear gradient of buffer C containing 40–200 mM NaCl and subjected to TEV proteolysis for 12 h. VDCC β_{2a}-containing fractions were pooled (80–100 mM NaCl) and loaded onto a pre-equilibrated gel filtration column (buffer G: 10 mM Tris (pH 8), 10 mM βME, 200 mM NaCl). The protein was eluted with buffer G. The pooled fractions were further processed as for β_3.

Subcloning, Expression, and Purification of VDCC β_{2a} Domain I—PCR was used to engineer EcoRI and BamHI restriction sites into the β_{2a} domain I construct. The oligonucleotide primers used for amplification of the β_{2a} domain I construct from the original β_{2a} plasmid were the following: sense primer E, 5′-GCGCGGATCCAGCCGTC-CATCCGATTCAGATGTG-3′; antisense primer F, 5′-GCGCGAATTCT-CACTTTGCTCTCTGTTCATGCTGTAG-3′. Subsequent subcloning was as described for VDCC β_3.

The β_{2a} domain I was expressed as for β_3. Purification was as follows. The soluble fraction of the crude extract was loaded on a pre-equilibrated Talon column (buffer A) and washed with buffer A, containing 75 mM imidazole. The protein was then eluted with buffer A, containing 150 mM imidazole, pooled, and subjected to TEV proteolysis for 12 h. The protein was then diluted 3-fold with 300 mM NaCl, loaded onto a pre-equilibrated (buffer H) hydroxylapatite column, and eluted with a linear gradient of H buffer 10–140 mM potassium phosphate (eluted at 70 mM potassium phosphate). The pooled fractions, with the addition of 10 mM βME, were loaded onto a pre-equilibrated gel filtration column (buffer G) and eluted with buffer G. The pooled fractions were processed as above.

Subcloning, Expression, and Purification of VDCC β_{2a} Domain II—PCR was used to engineer EcoRI and BamHI restriction sites into the β_{2a} domain II construct. The oligonucleotide primers used for amplification of the β_{2a} domain II construct from the original β_{2a} plasmid were the following: primer G, sense 5′-GCGCGGATCCCACTCCAAA-GAGAAAAGAATGCCC-3′; antisense primer I, 5′-GCGCGAATTCT-CAAAGGAGAGGGTTGGGGAGATTGCT-3′. PCR product was ligated into a doubly digested (EcoRI and BamHI) pET43.1a (Novagen) plasmid, thereby encoding a C-terminal fusion to the NusA protein with a His$_6$ tag and thrombin site separating the two. A modified pET43 (His$_8$ followed by a TEV cleavage sequence was inserted between the pET43 SpeI and BamHI sites) was also prepared to express domain II in the same way as with the commercial pET43.

The β_{2a} domain II was expressed as above. Purification of the NusA-domain II fusion proceeded as follows. The soluble fraction of the crude extract was loaded on a pre-equilibrated Ni-CAM column (buffer B) and washed with buffer B, containing 5 mM imidazole. The protein was then eluted with buffer B, containing 30 mM imidazole, loaded on a pre-equilibrated (H buffer) hydroxylapatite column and eluted with a linear gradient of buffer H 10–250 mM potassium phosphate (eluted at 100 mM potassium phosphate). The protein was then subjected to thrombin (Sigma) proteolysis (5 units/mg of fusion protein) for 14 h. The cleaved protein was diluted 2-fold and applied to a pre-equilibrated Q-Sepharose column with phosphate-buffered saline. The flowthrough fractions were pooled, divided into aliquots, and flash-frozen in liquid N_2.

Subcloning, Expression, and Purification of VDCC β_{2a} Removable Linker Core—Subcloning was stepwise. First, pre-digested PCR product encoding domain I was ligated into EcoRI- and BamHI-digested pET21d plasmid. Next, pET21d-domain I plasmid was prepared and digested with EcoRI and NotI for ligation with a pre-digested PCR

product encoding domain II. Finally, PCR product, encoding the linker between domains I and II and two TEV proteolysis sites at both ends, was singly digested with EcoRI and ligated into pre-digested EcoRI vector, now containing both domain I and domain II. Positive clones containing the insert in the correct orientation were identified using restriction analysis and sequencing.

PCR was used to engineer EcoRI, BamHI, and NotI restriction sites into the β_{2a} domain I and domain II encoding fragments. The oligonucleotide primers used for amplification of the β_{2a} domain I fragment from the original β_{2a} plasmid were the following: sense primer E, 5′ listed above; antisense primer J, 5′-CGCGGAATTCCTTTGCTCTCT-GTTCATGCTGTAG-3′.The oligonucleotide primers used for amplification of the β_{2a} domain II fragment from the original β_{2a} plasmid were the following: Sense primer K, 5′-CGGAATTCAAGCTTCACTCCAAA-GAGAAAAGAATGCCC-3′; antisense primer L, 5′-TTATACTAGCGGC-CGCTCAAAGGAGAGGGTTGGGGAGATT-3′. The oligonucleotide primers used for amplification of the β_{2a} linker fragment with the addition of two TEV sites from the original β_{2a} plasmid were the following: sense primer M, 5′-CGCGGAATTCGAAAACCTGTACTTTC-AGGGCCAAGGGAAATTCTACTCCA-3′; antisense primer N, 5′-CGCGGAATTCGCCCTGAAAGTACAGGTTTTCGGGTGACGTTAC-ACTGTTT-3′.

The VDCC β_{2a} removable linker core was expressed as above. The soluble fraction of the crude extract was loaded onto a pre-equilibrated Ni-CAM column (buffer B) and washed with buffer B, containing 5 mM imidazole. The protein was then eluted with buffer B, containing 150 mM imidazole, pooled and diluted 2-fold, followed by loading onto a pre-equilibrated hydroxylapatite column (H buffer). Protein was eluted with a linear gradient of H buffer (10–250 mM potassium phosphate) at about 120 mM potassium phosphate. Pooled fractions were diluted 4-fold and subjected for 12 h to TEV protease. 10 mM βME was added to the sample and loaded onto a pre-equilibrated gel filtration column (G buffer). Protein was eluted with buffer G. The pooled fractions were processed as above.

Limited Proteolysis of VDCC β_{2a} and β_3 Subunits—Papain (20 μg/ml) (Sigma-Aldrich) was activated for 30 min in activation buffer (1.25 mM EDTA, 6.25 mM cysteine, 62.5 mM βME, at pH 7) and added to 3 mg/ml VDCC β_3 or β_{2a} in a 1:20 dilution. The final ratio of papain to β protein was 1:3000. Trypsin (60 μg/ml) was added to 3 mg/ml β_3 in a 1:20 dilution, giving a final ratio of protease to protein of 1:1000. Reactions were performed on ice. Proteolysis progress (at different time intervals) was monitored by SDS-PAGE. Proteolysis products were purified for further analysis by HPLC reverse phase chromatography using a C4 column (Vydac) with a shallow acetonitrile gradient 30–80% (both solvents were supplemented with 0.05% trifluoroacetic acid).

AID Peptide Binding Assays—Fluorescence polarization was used to determine the equilibrium dissociation constant (K_D) for the interaction between a fluorescein-labeled AID peptide and various purified VDCC β constructs. The synthetic peptide was purified by HPLC reverse phase chromatography using a C18 column (Vydac) with a shallow acetonitrile gradient 20–80% (both solvents were supplemented with 0.05% trifluoroacetic acid). Its sequence is derived from the AID motif of the Ca$_V$1.1 I–II linker and is as follows: fluorescein-GGQQLEEDLRGYN-SWITQGE-COOH. A mutant peptide, fluorescein-GGQQLEEDLRG-SNSWITQGE-COOH was prepared, in addition. Increasing concentrations of protein were incubated with 0.5 nM labeled peptide for 10 min in the dark at room temperature. Polarization measurements were taken with an ISS K2 fluorescence spectrophotometer at excitation and emission wavelengths of 492 and 520 nm, respectively, at 20 °C, maintained by a temperature-controlled water bath. Polarization measurements were made with integration times on the order of 20 s, achieving a standard deviation of 5% of signal. Binding isotherms for the various samples were measured three independent times. Binding data were analyzed in SigmaPlot (SPSS) by nonlinear regression used to fit a binding function as defined by the following equation,

$$\Delta P = \frac{B_{max} X}{K_D \cdot X} \qquad \text{(Eq. 1)}$$

where X is the concentration of free ligand, ΔP is the change in fluorescence polarization of the fluorophore (the baseline polarization of the labeled peptide alone was subtracted), B_{max} is the maximum change in polarization upon saturation, and K_D is the concentration of ligand required to reach half-maximal binding.

CD Spectroscopy—All CD measurements were performed with an Aviv CD spectrometer model 202. Spectra were measured over the range of 280–180 nm at a scan rate of 1 nm/s. For all measurements, a cell with 0.1-mm path length was used. Each spectrum is an average of
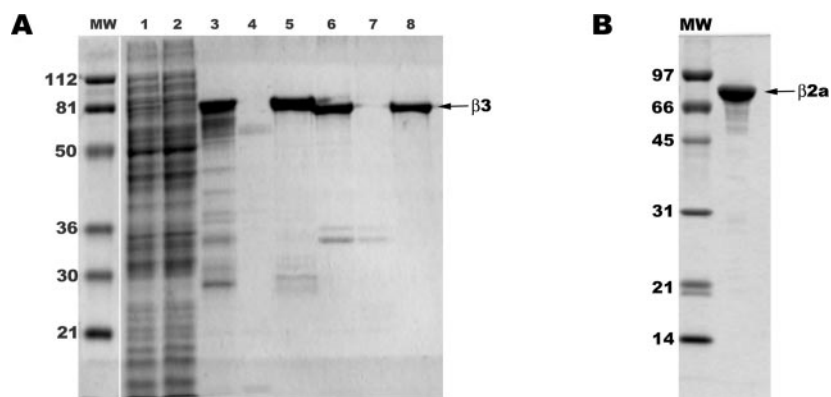
FIG. 2. **Purification of recombinant, full-length VDCC β proteins.** *A*, SDS-PAGE of VDCC β_3 purification in its various stages; *MW*, molecular weight markers (kDa); *lane 1*, soluble fraction of the crude lysate; *lane 2*, metal chelate column flowthrough fraction; *lane 3*, metal chelate column eluate fraction (first major purification step); *lane 4*, ion-exchange column flowthrough fraction; *lane 5*, ion-exchange column eluate fraction (second major purification step); *lane 6*, protein after TEV digestion, which removes a 26-residue N terminus, including the histidine tag, producing a distinct mobility shift; *lane 7*, hydroxylapatite column flowthrough fraction; *lane 8*, hydroxylapatite column eluate (final major purification step). *B*, SDS-PAGE of purified VDCC β_{2a}; *MW*, molecular weight markers (kDa); *neighboring lane*, gel-filtration column eluate (final major purification step) after concentration.

4 scans. The raw data were corrected by subtracting the contribution of the buffer to the CD signal. Data were smoothed and converted to molar ellipticity units. The measurements were taken at a constant temperature of 20 °C, with an approximate protein concentration of 35 μM. More precise concentration of protein was obtained using the predicted extinction coefficient of the proteins and their 280-nm absorbance. The proteins' molar extinction coefficients ($M^{-1}cm^{-1}$) at 280 nm were: β_3, 52,300; β_{2a}, 39,760; and β_{2a}-linkerless core, 24,870. The difference spectrum (full-length β_{2a}-linkerless core) was calculated according to a previous study (25). Deconvolution calculations were computed with CDNN (26) using the 33 data basis set.

Electrophysiology—Preparation of *Xenopus laevis* oocytes, injection of mRNA of VDCC subunits, and electrophysiological recording and analysis were performed as described previously (27). The negative control group consisted of oocytes expressing $Ca_V1.2$ (α_1C) subunit only by mRNA injection followed by injection of protein buffer (PB). The positive control group consisted of oocytes expressing α_1C and β_3 subunits by mRNA injection, followed by injection of protein buffer (PB). The oocytes of experimental groups were injected with α_1C mRNA followed by injection of VDCC β proteins, 2 days after the mRNA injection. Injection of protein (0.4 μg of protein per oocyte) was performed similarly as mRNA injection. Oocytes injected with VDCC β proteins were incubated one more day, and the expressed calcium channel currents were recorded using the two-electrode voltage-clamp technique.

<div align="center">RESULTS</div>

Expression and Purification—Using a T7 expression system, an *E. coli* BL-21 derivative cell line that allows for fine tuning IPTG induction by better controlling IPTG concentration, and low temperature growths, we obtained overexpression of soluble, full-length rat VDCC β_3. In addition, we subcloned and expressed the rabbit β_{2a} isoform in the same system. The expression vectors encode a histidine tag on the N terminus, followed by a TEV protease site and the ensuing desired coding sequence. We have found that VDCC β_{2a} manifests robust expression. β_3 expression is not exceptional.

Our purification schemes for the VDCC β isoforms vary. However, all utilize as a first step subsequent to lysis, metal chelate resin chromatography to isolate the His-tagged target proteins. This first step usually produces protein that is greater than 80–85% homogeneous. Histidine tags are removed by cleavage with TEV protease. The TEV protease is highly specific and does not cleave other sites on the protein. Full-length VDCC β_3 is highly sensitive to proteolysis. Therefore, efficient and rapid chromatographic processing has proven essential and has been applied systematically. The full-length proteins are shown in Fig. 2. The bacterial expressed recombinant proteins are both electrophysiologically and biochemically active (see below).

Limited Proteolysis—An important and classic method of probing protein structure is limited proteolysis (for a review see Ref. 28). The goal here is determination of domain structure. The premise of the method assumes that flexible and exposed regions of the protein are available to the protease and thus subject to hydrolysis.

We subjected both β_{2a} and β_3 recombinant full-length proteins to such an analysis using both papain, a highly nonspecific protease, and trypsin, a more specific protease. The time-course results for limited digestion by papain are shown in Fig. 3. Early in the time course, a stable polypeptide emerged that runs as a fragment of ~40 kDa. Subsequently, this fragment is further digested such that after 16 h, two stable fragments remain, one of higher mobility and another of medium mobility. Both isoforms basically follow the same pattern (β_{2a} seems to have an intermediate fragment). Having established a set of stable polypeptides, we sought to identify them. Preparative limited proteolyses of VDCC β_3 were performed, and at the appropriate times the reaction was stopped by flash freezing with liquid N_2. The samples were then applied to a reverse phase C4 HPLC column and separated by an acetonitrile gradient. The separated fragments were sent for mass spectrometric and N-terminal peptide sequencing analyses.

Electrospray mass spectrometry gave masses of 13,198 and 23,938 Da for the two stable fragments. We note that both fragments migrate anomalously on SDS-PAGE gels, and this has been a consistent feature of β_3 and β_{2a} proteins to varying degrees. N-terminal sequencing of these fragments indicated that the smaller one primarily began at residue 23, whereas the larger fragment began at residue 158. Combining these data allowed us to demarcate the boundaries of these stable domains. The smaller fragment is defined from 23 to 138 of the β_3 sequence and designated domain I, whereas the larger fragment is defined from 158 to 371 and designated domain II. The β_{2a} domain definitions are 25–146 and 204–423 for domains I and II, respectively, as determined by sequence alignment to the β_3 boundaries. The domain definitions conform well with earlier definitions based on homology alone.

We then sought to identify the early proteolytic 40-kDa fragment, thinking that it may simply be composed of domains I and II with a linker. MALDI-MS analyses of this polypeptide gave a cluster of masses centered around 39,420 Da. This mass is consistent with a fragment extending from residue 21 to 370 and fits as well with the mass spectrometry and peptide sequencing results of the stable domains. Moreover, the stable
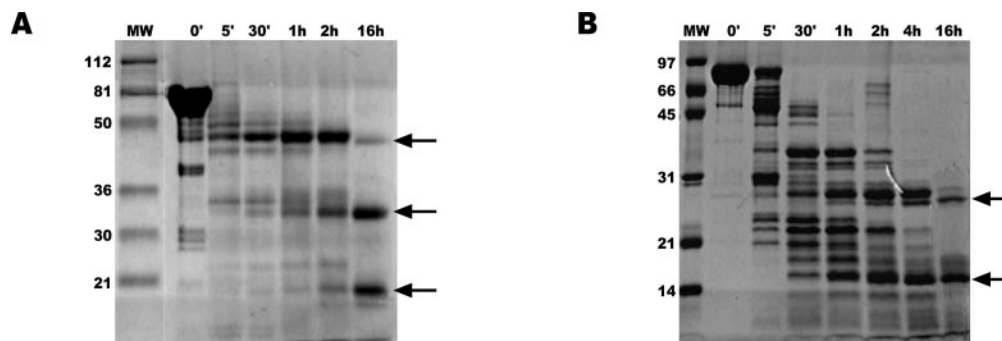
F<small>IG</small>. 3. **Limited proteolyses of full-length VDCC β proteins.** *A*, β_3 was incubated with activated papain at a ratio of 3000:1 on ice in 10 m<small>M</small> Tris, pH 8, 200 m<small>M</small> NaCl, 5–10 m<small>M</small> βME. Aliquots were taken from the reaction at the indicated times, SDS sample buffer was added, and samples were boiled and analyzed later by SDS-PAGE, as shown. *B*, β_{2a} incubated with activated papain and analyzed as for β_3. *Arrows* indicate the protease-resistant fragments.

domains are derivatives of this early fragment as discerned by the time-course results, requiring them to be equal or smaller than the early fragment. We conclude that the large fragment is a core protein. Further support for this structural division, *i.e.* two domains with a flexible connecting linker, came from limited proteolysis of a recombinant protein, whose ends were engineered based on homology of the VDCC β family (see Fig. 1, *predicted core*). This limited proteolysis resulted in two fragments of the same size as the long term proteolyses of the full-length proteins (data not shown).

Domain Analysis—Having defined two stable domains of β, we chose to determine whether they interacted or rather were inert with regards to each other and behaved as pearls on a string. Constructs expressing His-tagged β_{2a} domain I alone and domain II as a C-terminal fusion protein with NusA were prepared (see Fig. 1). His-tagged domain I was mixed with domain II, which had been isolated away from the fusion partner NusA and shown to bind in a pull-down assay, indicating stable association of the two domains (Fig. 4*A*).

In addition, chromatographic experiments suggest that β_{2a} domains I and II stably interact. Gel filtration analysis of domain I alone gives an elution volume of 93 ml on a Superdex 200 size-exclusion column. When purified removable linker core protein (Fig. 1) was digested by TEV so that the domains were no longer covalently linked, to give linkerless core, and then run out on the identical column, both domains I and II co-eluted at an elution volume of 83 ml (Fig. 4*B*). The significant shift in elution volume for domain I and coelution of both domains strongly supports association of domains I and II. The solution conditions, 200 m<small>M</small> NaCl and 10 m<small>M</small> βME, for this chromatography run rule out nonspecific or adventitious association.

Circular Dichroism Spectroscopy—We measured CD spectra of several VDCC β forms, and they are shown in Fig. 5. The spectra of the full-length β_3 and β_{2a} proteins are similar indicating comparable secondary structure. Furthermore, these spectra indicate that the proteins are of a mixed α-helix/β-sheet type, as seen by visual inspection of the curves as well as by deconvolution calculations. The calculations point to ~35% sheet and 15% helix. A comparison of β_3 and the β_{2a} linkerless core spectra shows a very strong resemblance between these two proteins. In addition, the difference spectrum between β_{2a} full-length protein and the β_{2a} linkerless core protein gives insight into the segments of protein outside of domains I and II, namely the N-terminal segment, the linker between domains, and the C-terminal segment. This spectrum points to a significant fraction of random coil structure as evidenced by the shift in minimum and magnitude toward 198 nm and diminution of the other minimum at 222 nm (25), consonant with the limited proteolysis results.

AID Binding Assay—To enable structure-function correlations regarding our domain analysis and to have a robust *in vitro* assay for further correlations with structural and electrophysiological experiments, we have developed a novel assay that measures binding of VDCC β proteins to an α_1 I–II linker-derived AID peptide. The assay employs fluorescence polarization measurements. AID peptides of 18- to 20-residue length were synthesized, and some of them were labeled with fluorescein attached at the N terminus. Labeled peptide was then titrated with increasing concentrations of β, and the fluorescence polarization emitted by the labeled peptide was determined. Fluorescence emission polarization is proportional to the rotational correlation time (tumbling) of the labeled molecule. Tumbling, in part, depends on the molecular volume, *i.e.* larger molecules have larger volume and slower tumbling, which in turn gives rise to increased polarization of emitted light. If the peptide associates with β, its effective molecular volume greatly increases, as evidenced by values of fluorescence emissions polarization. Equilibrium isotherm titrations were performed with full-length β_{2a} and linkerless core β_{2a}. The binding curves are shown in Fig. 6 (*A* and *B*). They indicate high affinity single site binding on the order of 6–15 n<small>M</small>. The binding is specific, because addition of unlabeled AID peptide lowers the polarization to basal levels, *i.e.* it effectively competes with the labeled peptide (data not shown). The assay was further validated by testing a mutant AID peptide, which has a single amino acid change (Tyr to Ser). The same mutant AID bound less than 5% of WT previously, using another *in vitro* binding assay system (29). Using our fluorescence assay, no binding of the mutant AID was detected at concentrations of up to 350 n<small>M</small> β_{2a} protein, where WT peptide has reached saturation binding.

We next used this binding assay to investigate which domains of β are required for association with the AID peptide (Fig. 6*C*). Our objective in this experiment was not to measure absolute affinities but rather to measure relative ones. First, binding of β_{2a} domain I was assessed. As can be seen, binding was negligible in the estimated concentration regime tested. Next, the NusA-domain II fusion, which contains a TEV protease site separating NusA and domain II, was incubated with TEV protease and the labeled peptide for 1 h and then fluorescence polarization was measured. As observed, domain II demonstrates significant binding affinity for the AID. In stage three, the β_{2a} domain I protein and the NusA-domain II fusion protein, again containing a TEV protease site separating NusA and domain II, were incubated with TEV protease and the labeled peptide for a period of 1 h, and then fluorescence polarization was assessed. The binding curve shows that the presumed domain I-domain II complex binds with even higher affinity. Because identical amounts of the various proteins were taken in the three stages of this experiment, the curves
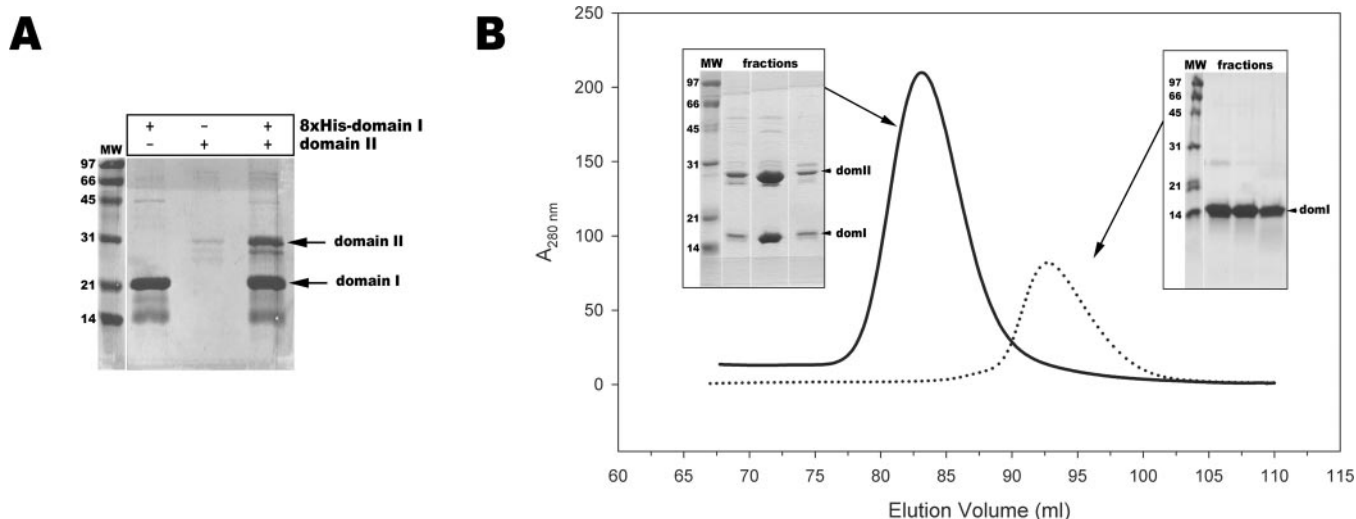
FIG. 4. **Domains I and II associate.** *A*, SDS-PAGE gel stained with Coomassie Blue of a pull-down assay. Domain I contains a polyhistidine tag with which it was immobilized, whereas domain II was without a tag. Protein input is indicated by the key above the gel. *Left lane*, domain I pulled down with metal-chelate resin; *center lane*, domain II pulled down with metal-chelate resin (there is a small degree of nonspecific binding to the resin); *right lane*, immobilized domain I after incubation with domain II for 20 min in phosphate buffer, pH 7, containing 300 mM NaCl. Protein input was on the order of 10 μg of protein. Beads were washed five times with buffer for all experiments. The output of domain II in the *right lane* is dramatically enhanced due to association with domain I. Relevant bands are labeled. *B*, gel-filtration chromatography elution profile of domain I alone (*dotted trace*) and linkerless core (*solid line*), after digestion with TEV protease to remove the linker. The *insets* show SDS-PAGE gels of the relevant central fractions from each peak. As can be easily discerned, domains I and II co-eluted in the *left-hand peak*. Relevant bands are labeled

FIG. 5. **Circular dichroism spectra of VDCC β proteins.** Each curve is labeled as per the legend. The *ordinate* is molar ellipticity units (deg cm^2 dmol^{-1}). Measurement details are described under "Experimental Procedures."
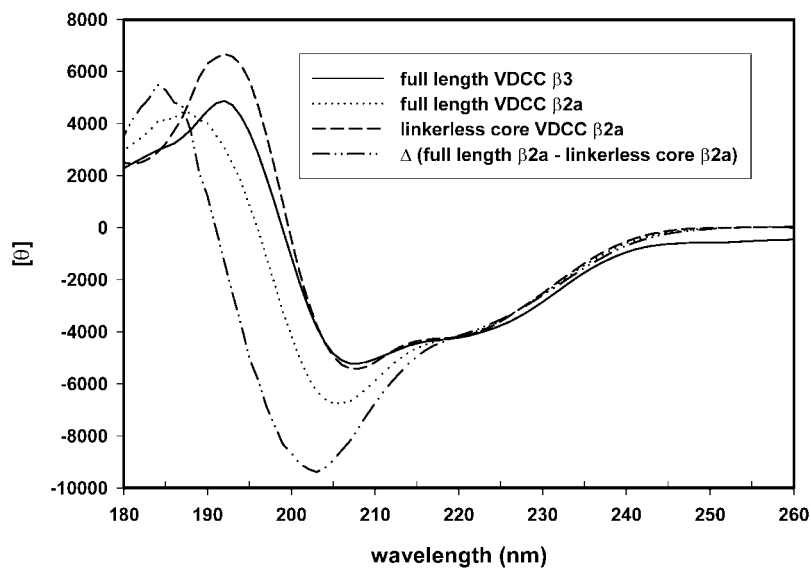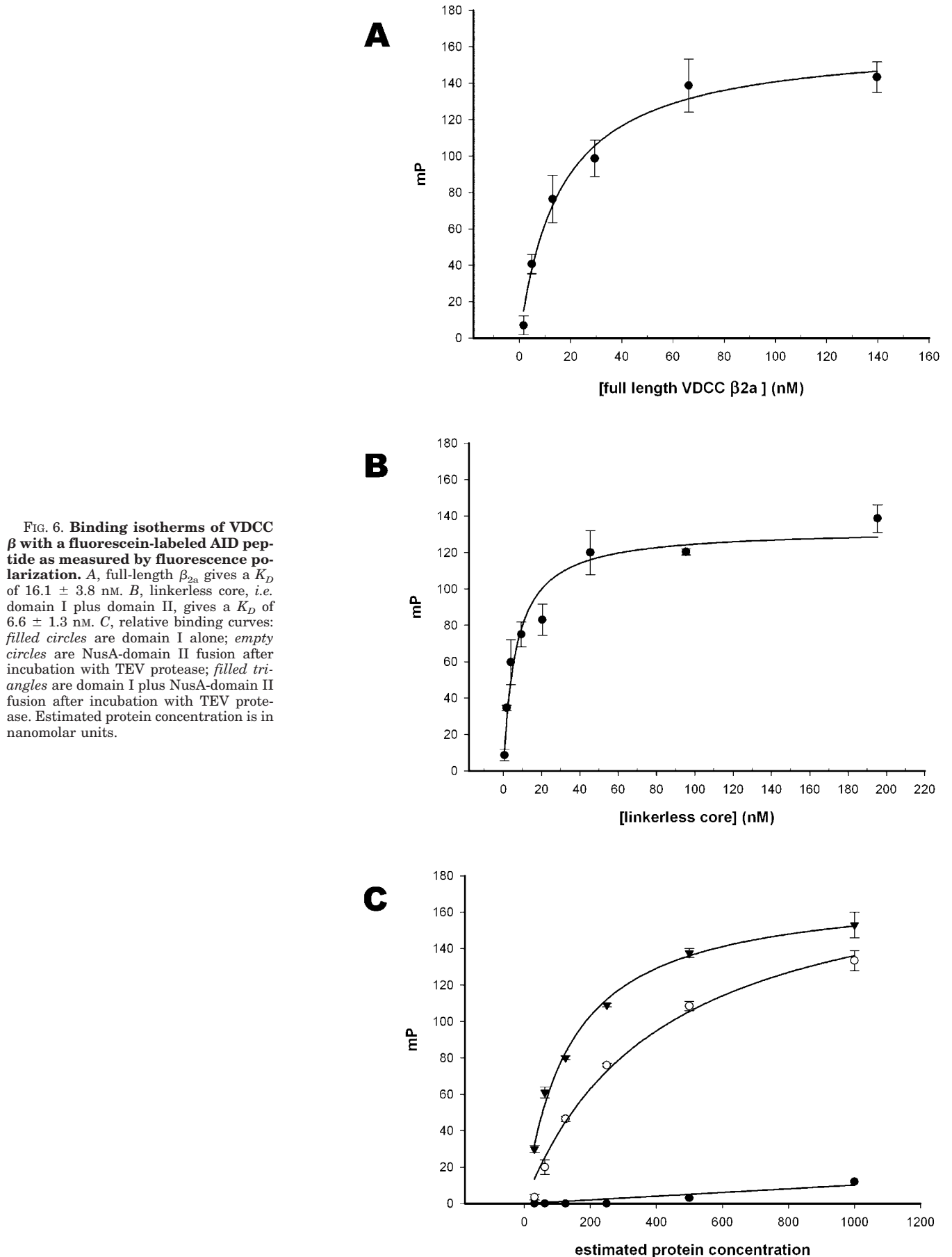
provide us with a reasonable relative measurement of binding for the different domains and their individual contributions. Thus, domain I does not bind by itself to the AID at high affinity, whereas domain II does. However, it is clear that domain I somehow contributes to the increased binding of the AID for the presumed domain I-domain II complex.

Electrophysiology—To assure that our bacterially expressed, recombinant proteins are physiologically active, we performed two-electrode voltage-clamp measurements of *Xenopus* oocytes expressing α_1 and microinjected with our protein samples. In the I–V plots of Ca$_v$1.2 currents (Fig. 7), we show an increase of current amplitude and shift of the steady-state activation by injection of β proteins (except domain I), demonstrating the functional activity of the β proteins. Data values and statistical analyses are described in Table I. The current amplitude in-

crease and change of steady-state activation are statistically significant in all experimental groups except a group injected with β_{2a} domain I protein.

Furthermore, the results show that the core protein electrophysiological activity corresponds well to full-length protein activity. In addition, the injection of purified domain I and domain II proteins prepared by proteolysis of full-length protein and subsequent purification, comparable to β_{2a} linkerless core protein from our *in vitro* experiments, still enabled significant changes in the current amplitude and activation shift in a qualitatively similar manner as native protein. It should be noted that the injected recombinant β_{2a} proteins were found subsequently to contain a mutation (P122R) due to the PCR subcloning. This mutation had no effect on the electrophysiological activity of the protein.
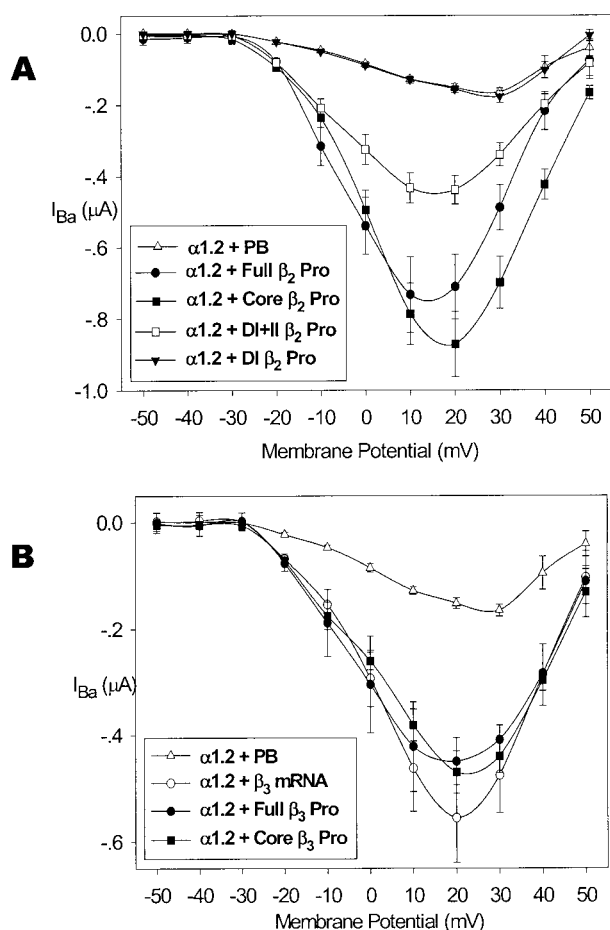
FIG. 6. **Binding isotherms of VDCC β with a fluorescein-labeled AID peptide as measured by fluorescence polarization.** *A*, full-length β_{2a} gives a K_D of 16.1 ± 3.8 nM. *B*, linkerless core, *i.e.* domain I plus domain II, gives a K_D of 6.6 ± 1.3 nM. *C*, relative binding curves: *filled circles* are domain I alone; *empty circles* are NusA-domain II fusion after incubation with TEV protease; *filled triangles* are domain I plus NusA-domain II fusion after incubation with TEV protease. Estimated protein concentration is in nanomolar units.

FIG. 7. **Functional assay of purified β proteins.** Physiological activities of the purified proteins were examined by two-electrode voltage clamp analysis of oocytes expressing VDCC by combination of mRNA and protein injection. *A*, VDCC consisted of $\alpha_{1.2}$ and β_2 proteins. *B*, VDCC consisted of $\alpha_{1.2}$ and β_3 proteins. *PB*, protein buffer; *Pro*, protein; *DI*, domain I; *DI+II*, domain I plus domain II prepared by proteolysis of full-length protein and subsequent purification.

DISCUSSION

Our limited proteolysis results, in conjunction with further analysis of the fragments by mass spectrometry and N-terminal sequencing, demonstrate experimentally for the first time the two-domain structure of the VDCC β family. The results correspond remarkably well with sequence analysis (Fig. 8), electrophysiological studies, and molecular modeling. Previous studies have divided the family into five domains, namely D1 corresponding to the N-terminal region, D2 (domain I in our work), D3 (the linker), D4 (domain II), and D5, the C-terminal region. Based on the studies described here, this division may be misleading, because D1, D3, and D5 do not likely represent authentic, independently folded domains for reasons elaborated below. Moreover, we posit that the domain structure applies to all members of the family, because at least two members, β_{2a} and β_3, exhibited parallel limited proteolysis results and because the domain ends coincide with sequence conservation boundaries. Buttressing this contention, the CD spectra of the two members have like features. These two structural domains seem to encode critical features of the functional activity of the β family, as summarized previously (18).

Studies of limited proteolysis have defined three major determinants of proteolytic susceptibility, namely exposure, flexibility, and sparse local interactions of the substrate protein (30). Protein regions with well defined secondary structure are rich in local interactions, preventing local unfolding and thus

proteolysis (31). In light of the limited proteolysis results, we conclude that regions N-terminal to domain I and C-terminal to domain II are mostly likely not highly structured when β is alone in solution, *i.e.* when VDCC β is not bound to α_1. This conclusion is supported by secondary structure prediction algorithms such as PredictProtein (32) and homology sequence analysis. In addition, the region linking domains I and II, dubbed the linker, was susceptible to digestion, suggesting that it too is not highly structured and quite flexible. Inspection of the linker's sequences argues that sections of the linker are unlikely to be structured due to their low sequence complexity (very highly rich in serines, with a high fraction of prolines and glycines as well) (33). Here again, the CD difference spectrum (full-length β_{2a}-linkerless core) is consistent with the notion that regions outside of domains I and II are mostly unstructured when not in complex with α_1. This difference spectrum represents a polypeptide not present in the linkerless core, *i.e.* regions other than domains I and II. It is most easily interpreted as showing significant random coil conformation. Furthermore, we argue that the close correspondence of β_{2a} linkerless core and β_3 spectra (see Fig. 5) emphasizes the nature of extra-domain regions. β_{2a} contains 122 more residues than β_3. These additions are located in the linker and C-terminal regions. On the other hand, β_3 is the smallest member of the family with the shortest N-terminal, linker and C-terminal regions. Thus, β_3 most closely resembles a minimal version of the β family as represented by the engineered β_{2a} linkerless core, explaining the strong resemblance of the two spectra.

The domain analysis led us to propose two working models for the domain structure of β (Fig. 9). One model postulates that the domains do not associate and a flexible linker tethers them together. Alternatively, the domains associate with each other in a stable manner and a flexible linker connects them but is not required for the domain association. Biochemical results, *i.e.* the pull-down assay and size-exclusion chromatography, rule out the former possibility.

From the biochemical binding data for the various protein forms, it appears that binding determinants for the AID reside primarily in domain II, as noted previously (22). Nevertheless, domain I makes a contribution (Fig. 6*C*), either directly, by facilitating interactions between the AID and domain II, or indirectly, by stabilizing domain II as a folded protein entity due to domain I-domain II complexation. The contribution is also discernible in the electrophysiological data measured earlier (22) where current amplitude is increased upon injecting mRNA encoding the equivalent of β core *versus* β domain II (see Fig. 4 in Ref. 22). Notably, the linker clearly does not contribute to AID binding (Fig. 6*B*). Removing it appears to improve β-AID association. That the linkerless core binds the AID with maximal affinity, lends support to the model that domains I and II stably interact and that the linker is not necessary for the structural integrity of the protein. Indeed, due to its sequence composition it may encode a PEST determinant for degradation of the protein and thus is important for regulation of β, not its biochemical and electrophysiological activities. Supporting this hypothesis, analysis of the VDCC β_{2a} sequence with PEST search algorithms (34) locates a sequence in the linker that is likely to be a good PEST candidate.

Two permutations arise in regard to AID binding: one, before complexation with the AID, β domains I and II are stably bound. Upon encountering the AID, a conformational change takes place and the two domains dissociate, with concomitant AID binding. Two, the domains remain stably bound together whether the AID associates or not. This second option does not rule out a conformational change on the part of β when complex formation with the AID occurs. Rather it negates a scenario

TABLE I
Electrophysiological parameters of the Ca$_v$1.2 oocyte expression plus protein microinjections

Values are presented as mean ± S.E.

Properties	$\alpha_{1.2}$	$\alpha_{1.2}+\beta_3$mRNA	$\alpha_{1.2}+$Fullβ_3Pro.	$\alpha_{1.2}+$Coreβ_3Pro.
Current amplitude (μA)				
I at 20 mV[a]	-0.15 ± 0.01	-0.56 ± 0.08^b	-0.47 ± 0.04^c	-0.45 ± 0.04^c
I at 30 mV	-0.16 ± 0.01	-0.48 ± 0.07^b	-0.44 ± 0.03^c	-0.41 ± 0.03^c
n	10	11	10	8
Steady-state activation parameters from the I–V curve				
$V_{1/2}$ (mV)	22.60 ± 4.22	10.67 ± 1.95^b	10.03 ± 3.36^d	10.65 ± 4.46^d
k (mV)	11.91 ± 0.84	9.08 ± 0.36^b	10.56 ± 0.42	10.06 ± 1.15
n	10	11	10	8

Properties	$\alpha_{1.2}+$Fullβ_2Pro.	$\alpha_{1.2}+$Coreβ_2Pro.	$\alpha_{1.2}+$d1+d2β_2Pro.	$\alpha_{1.2}+$d1β_2Pro.
Current amplitude (μA)				
I at 20 mV	-0.71 ± 0.09^b	-0.87 ± 0.09^c	-0.44 ± 0.04^c	-0.16 ± 0.01
I at 30 mV	-0.49 ± 0.06^b	-0.70 ± 0.07^c	-0.34 ± 0.03^b	-0.18 ± 0.02
n	11	11	12	9
Steady-state activation parameters from the I–V curve				
$V_{1/2}$ (mV)	3.68 ± 0.33^c	6.84 ± 0.83^c	3.24 ± 0.93^c	24.00 ± 3.01
k (mV)	8.48 ± 0.53^c	8.43 ± 0.23^c	9.49 ± 0.92	12.18 ± 0.49
n	11	11	12	9

[a] I, current; V, potential; $V_{1/2}$, membrane potential for half-maximal activation; k, slope factor; n, cell number; *Pro.*, protein; d, domain.
[b] $p < 0.01$ (in terms of $\alpha_{1.2}$).
[c] $p < 0.001$ (in terms of $\alpha_{1.2}$).
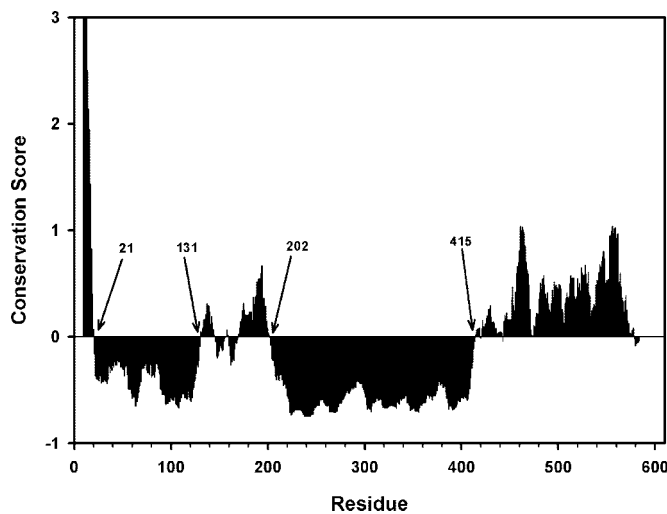[d] $p < 0.05$ (in terms of $\alpha_{1.2}$).

FIG. 8. **VDCC β protein family sequence conservation.** 24 protein sequences of VDCC β were selected from the NCBI data base, based on a search with BLAST. Splice variants were removed, and the selection included several invertebrate and vertebrate sequences. These sequences were run on the ConSeq server (available at conseq.bioinfo.tau.ac.il), which uses the Max4Site algorithm (35) to compute sequence conservation scores. Scores account for evolutionary distances and are normalized to units of standard deviation. Zero represents the average evolutionary rate, and less than 0 indicates increasing conservation. The scores were then averaged in a window of ±5 residues (*i.e.* 11 total residues) for every residue and plotted as seen in the histogram. *Arrows* indicate the residue numbers of blocks of significant conservation. These blocks correspond quite well with the biochemically defined domains I and II. The reference sequence for numbering is rabbit β_{2a}.

FIG. 9. **Schematic of alternative models for VDCC β domain configurations.**

flexible, solvent-exposed, and possibly unstructured. They are unnecessary for β protein binding to the primary anchor site in VDCC α_1 subunits. Although domain II contains the function of current amplitude amplification and the voltage activation shift attributed previously to β function, domain I potentiates this facility (22). We speculate that these domains provide a stable structural center for β functionality. The remaining sequences (N terminus, C terminus, and linker) of the β subunit will then be positioned by way of the attachment of the core to the AID to interact with other surfaces on α_1 (10, 11), influencing other important functional activities such as activation and inactivation kinetics (18). In addition, we have introduced a novel and robust *in vitro* binding assay for VDCC β and the AID, which may be readily used for screening compounds that inhibit or modulate this critical interaction.

wherein such a conformational switch results in dissociation between the two β domains. Interestingly, pull-down experiments in the presence of the AID peptide showed little difference from assays performed in its absence, arguing that the two domains do not dissociate upon AID binding (data not shown).

In summary, we have delineated, based on protein biochemistry, two *bona fide* folded domains with mixed helix/sheet secondary structure in VDCC β proteins. The domains mutually interact in a stable manner. Extraneous sequences, including the linker between domains, would appear to be highly
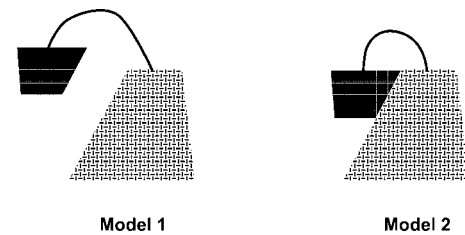
REFERENCES

1. Nakai, J., Tanabe, T., Konno, T., Adams, B., and Beam, K. G. (1998) *J. Biol. Chem.* **273,** 24983–24986
2. Bers, D. M., and Perez-Reyes, E. (1999) *Cardiovasc. Res.* **42,** 339–360
3. Finkbeiner, S., and Greenberg, M. E. (1998) *J. Neurobiol.* **37,** 171–189
4. Sheng, M., Thompson, M. A., and Greenberg, M. E. (1991) *Science* **252,** 1427–1430
5. Catterall, W. A. (1996) *J. Bioenerg. Biomembr.* **28,** 219–230

6. Takahashi, M., and Catterall, W. A. (1987) *Biochemistry* **26,** 5518–5526
7. Birnbaumer, L., Qin, N., Olcese, R., Tareilus, E., Platano, D., Costantin, J., and Stefani, E. (1998) *J. Bioenerg. Biomembr.* **30,** 357–375
8. Pragnell, M., De Waard, M., Mori, Y., Tanabe, T., Snutch, T. P., and Campbell, K. P. (1994) *Nature* **368,** 67–70
9. Leung, A. T., Imagawa, T., Block, B., Franzini-Armstrong, C., and Campbell, K. P. (1988) *J. Biol. Chem.* **263,** 994–1001
10. Tareilus, E., Roux, M., Qin, N., Olcese, R., Zhou, J., Stefani, E., and Birnbaumer, L. (1997) *Proc. Natl. Acad. Sci. U. S. A.* **94,** 1703–1708
11. Walker, D., Bichet, D., Campbell, K. P., and Dewaard, M. (1998) *J. Biol. Chem.* **273,** 2361–2367
12. Walker, D., Bichet, D., Geib, S., Mori, E., Cornet, V., Snutch, T. P., Mori, Y., and De Waard, M. (1999) *J. Biol. Chem.* **274,** 12383–12390
13. Canti, C., Page, K. M., Stephens, G. J., and Dolphin, A. C. (1999) *J. Neurosci.* **19,** 6855–6864
14. Stephens, G. J., Page, K. M., Bogdanov, Y., and Dolphin, A. C. (2000) *J. Physiol.* **525,** 377–390
15. Lacerda, A. E., Kim, H. S., Ruth, P., Perez-Reyes, E., Flockerzi, V., Hofmann, F., Birnbaumer, L., and Brown, A. M. (1991) *Nature* **352,** 527–530
16. Singer, D., Biel, M., Lotan, I., Flockerzi, V., Hofmann, F., and Dascal, N. (1991) *Science* **253,** 1553–1557
17. Varadi, G., Lory, P., Schultz, D., Varadi, M., and Schwartz, A. (1991) *Nature* **352,** 159–162
18. Walker, D., and De Waard, M. (1998) *Trends Neurosci.* **21,** 148–154
19. Yamaguchi, H., Hara, M., Strobeck, M., Fukasawa, K., Schwartz, A., and Varadi, G. (1998) *J. Biol. Chem.* **273,** 19348–19356
20. Brice, N. L., Berrow, N. S., Campbell, V., Page, K. M., Brickley, K., Tedder, I., and Dolphin, A. C. (1997) *Eur. J. Neurosci.* **9,** 749–759
21. Bichet, D., Cornet, V., Geib, S., Carlier, E., Volsen, S., Hoshi, T., Mori, Y., and De Waard, M. (2000) *Neuron* **25,** 177–190
22. De Waard, M., Pragnell, M., and Campbell, K. P. (1994) *Neuron* **13,** 495–503
23. Hanlon, M. R., Berrow, N. S., Dolphin, A. C., and Wallace, B. A. (1999) *FEBS Lett.* **445,** 366–370
24. Kapust, R. B., and Waugh, D. S. (1999) *Protein Sci.* **8,** 1668–1674
25. Ausio, J., Toumadje, A., McParland, R., Becker, R. R., Johnson, W. C., Jr., and van Holde, K. E. (1987) *Biochemistry* **26,** 975–982
26. Bohm, G., Muhr, R., and Jaenicke, R. (1992) *Protein Eng.* **5,** 191–195
27. Kang, M. G., Chen, C. C., Felix, R., Letts, V. A., Frankel, W. N., Mori, Y., and Campbell, K. P. (2001) *J. Biol. Chem.* **276,** 32917–32924
28. Hubbard, S. J. (1998) *Biochim. Biophys. Acta* **1382,** 191–206
29. Witcher, D. R., De Waard, M., Liu, H., Pragnell, M., and Campbell, K. P. (1995) *J. Biol. Chem.* **270,** 18088–18093
30. Hubbard, S. J., Beynon, R. J., and Thornton, J. M. (1998) *Protein Eng.* **11,** 349–359
31. Fontana, A., Polverino de Laureto, P., De Filippis, V., Scaramella, E., and Zambonin, M. (1997) *Fold Des.* **2,** R17–R26
32. Rost, B. (1996) *Methods Enzymol.* **266,** 525–539
33. Romero, P., Obradovic, Z., Li, X., Garner, E. C., Brown, C. J., and Dunker, A. K. (2001) *Proteins* **42,** 38–48
34. Rechsteiner, M., and Rogers, S. W. (1996) *Trends Biochem. Sci.* **21,** 267–271
35. Pupko, T., Bell, R. E., Mayrose, I., Glaser, F., and Ben-Tal, N. (2002) *Bioinformatics* **18,** Suppl. 1, S71–S77